Endothelial cell malfunction in unruptured intracranial aneurysm lesions revealed using a 3D-casted mold

Isao Ono, MD[1, 2, 3)*], Yu Abekura, MD. PhD[1, 2, 3)*], Akitsugu Kawashima, MD. PhD[4)], Mieko Oka[1, 3, 5)], MD. PhD, Akihiro Okada, MD[1, 2, 3)], Shintaro Hara, PhD[6)], Susumu Miyamoto, MD. PhD[2)], Hiroharu Kataoka, MD. PhD[7)], Akira Ishii, MD. PhD[2)], Kimiko Yamamoto, PhD[8)], Tomohiro Aoki, MD. PhD[1, 3)]

*: equally contributed to the present study

1) Department of Molecular Pharmacology, Research Institute, National Cerebral, and Cardiovascular Center, Osaka 564-8565, Japan

2) Department of Neurosurgery, Kyoto University Graduate School of Medicine, Kyoto 606-8507, Japan

3) Core Research for Evolutional Science and Technology (CREST) from Japan Agency

for Medical Research and Development (AMED), National Cerebral and Cardiovascular Center, Osaka 564-8565, Japan

4) Department of Neurosurgery, Tokyo Women's Medical University Yachiyo Medical Center, Chiba 276-8524, Japan

5) Department of Neurosurgery, Tokyo Women’s Medical University, Tokyo 162-8666, Japan

6) Department of Bioengineering, Graduate School of Medicine, The University of Tokyo, Tokyo 113-0033, Japan

7) Department of Neurosurgery, Research Institute, National Cerebral, and Cardiovascular Center, Osaka 564-8565, Japan

8) System Physiology, Department of Biomedical Engineering, Graduate School of Medicine, The University of Tokyo, Tokyo 113-0033, Japan

Corresponding author; Tomohiro Aoki

Department of Molecular Pharmacology, Research Institute, National Cerebral, and Cardiovascular Center, 6-1 Kishibe-Shinmachi, Suita City, Osaka 564-8565, Japan

TEL: +81-6-6170-1070 (ext. 41023) / FAX: +81-6-6170-1416

E-mail: tomoaoki@ncvc.go.jp

Abstract

Intracranial aneurysm (IA), a socially important disease, is a major cause of subarachnoid hemorrhage. It is a chronic inflammatory disease in the intracranial arterial walls triggered and modified by hemodynamic force loading. Because the IA lesion morphology is complex, the blood flow conditions loaded on endothelial cells in each part of the lesion *in situ* vary greatly. We created a 3D-casted mold of the human unruptured IA lesion and cultured endothelial cells on this model, which was then perfused with culture media to model physiological flow conditions. Then, gene expression profiles of endothelial cells in each part of the IA lesion were analyzed. Comprehensive gene expression profile analysis revealed similar gene expression patterns in endothelial cells from each part of the IA lesion. Gene ontology analysis revealed endothelial cell malfunction within the IA lesion. Histopathological examination by electron microscopy and immunohistochemical analysis indicated that endothelial cells within IA lesions are damaged and dysfunctional. Thus, our findings revealed endothelial cell malfunction in IA lesions and provided new insights into IA pathogenesis.

Key Words: 3D-casted mold, endothelial cell, hemodynamic force, intracranial aneurysm

Introduction

Intracranial aneurysms (IAs) are lesions characterized morphologically by regional bulging of intracranial arteries, mainly at bifurcation sites. Histopathologically, they can be distinguished by degenerative changes in the arterial wall, typically a loss of medial smooth muscle cells and inflammatory infiltrates. IA affects 1 % ~ 5 % of the general population and is the primary cause of subarachnoid hemorrhage, the most severe form of stroke with a mortality rate of up to 50 % [1-5]. Given the poor prognosis after the onset of subarachnoid hemorrhage, preventing IA is important. However, no drug therapy is currently available to prevent its progression and rupture; therefore, many patients cannot receive effective treatment [6]. Understanding IA pathogenesis will help to identify novel therapeutic targets, allow the development of therapies against identified targets, and improve public health.

Because of the nature of vascular diseases and the unique morphological character of arterial bifurcations where IAs are formed, the pathophysiology of IAs is greatly influenced by the hemodynamic force exerted by blood flow and the heartbeats. Many studies using computational fluid dynamics (CFD) support this notion. Thus, IA is currently considered a hemodynamic force-mediated disease [7-16]. Among hemodynamic factors, the relationship between wall shear stress (WSS) and disease

development has been extensively studied. IA lesions are induced by a high WSS loading on a bifurcation site. However, the region that undergoes lesion enlargement after initiation is associated with low WSS. Furthermore, turbulence in blood flow may be a potent regulator that promotes IA development. Indeed, an *in vitro* study using cultured endothelial cells showed that turbulent flow exacerbates chemoattractant signals that initiate inflammatory cell infiltration [8].

Although the gross flow pattern is described in the above study, the actual flow conditions in each part of the IA lesion may vary significantly *in situ*. However, the precise molecular events that occur in endothelial cells at each part of the lesion in response to complex hemodynamic conditions remain to be elucidated. The molecular events in each part of the lesion that occur in response to specific flow conditions *in situ* underlie IA pathophysiology. Thus, clarifying such events is essential for understanding disease pathogenesis. Furthermore, understanding the response of each endothelial cell to hemodynamic force in each part of the lesion will provide knowledge about disease pathogenesis and the machinery regulating the mechano-sensing by endothelial cells.

In the present study, we prepared a 3D-casted model using morphological data from a human unruptured IA lesion. We also examined the gene expression profile of endothelial cells cultured on each part of the cast.

Methods

Study Approval

Data were collected from human patients by 3D-rotation angiography and approved by the local ethical committee at Kyoto University Graduate School of Medicine (Approved number #R1150), where data were processed.

All animal care, use, and experiments complied with the National Institutes of Health Guide for the Care and Use of Laboratory Animals and the Animal Research Reporting In Vivo Experiments (ARRIVE) guideline. Experimental animal procedures were approved by the Institutional Animal Care and Use Committee of National Cerebral and Cardiovascular Center (approval number #19036, #20003 and #21015).

Human-unruptured IA samples and control arterial walls from superficial temporal artery were obtained during neck clipping after obtaining written informed consent. The use of human samples was approved by the Ethics Committee at Kyoto University Graduate School and Faculty of Medicine (Approval Number #E2540 and #R0601), National Cerebral and Cardiovascular Center (Approval Number #M29-050, #R21012 and #R20126), and Tokyo Women's Medical University Yachiyo Medical Center (Approval Number #4106) where samples were prepared.

Construction of a 3D-casted mold of a human IA lesion with its parent artery and daughter arteries

A 3D-casted mold of a human IA lesion was made using hydrophilic silicon (#TSE3450, Momentive Performance Materials Japan, Tokyo, Japan) based on the morphological data obtained using 3D-rotation angiography from a human patient with an IA lesion at the bifurcation site of the middle cerebral artery.

Cell culture and cell-seeding on a 3D-casted mold and perfusion experiments

Primary culture of endothelial cells from the human umbilical artery (HUAEC) was purchased from Cell Applications (#C-12202, Lot#395Z010.2, San Diego, CA). Cells were cultured using a special medium from Cell Applications. The 3D-casted mold was coated with collagen type I (Cellmatrix Type I-P, Nitta Gelatin, Osaka, Japan), and primary cultured endothelial cells were seeded on the mold surface. After 12 h, the 3D-casted mold was perfused with a complete culture medium in a pulsatile manner (55 ml/min, 60 Hz, 3 h). Then, the cells were fixed with ice-cold 4 % paraformaldehyde solution.

RNA sequencing and data analyses

RNA-seq libraries were prepared from the fixed cells using SMART-Seq® Single Cell PLUS Kit (#R400751, TAKARA BIO INC., Shiga, Japan). Paired-end sequencing (2 × 75 base pair) was performed on a NextSeq500 (Illumina, Inc., San Diego, CA). The reads were aligned to the UCSC hg38 genome using the CLC genomics workbench (version 11, QIAGEN, Venlo, Netherlands). Differential expression analyses, including principal component analysis and gene ontology (GO), were performed using iDEP.93 (http://bioinformatics.sdstate.edu/idep/). Genes whose expression reached a fold change greater than 2.0 or less than 0.5 in cells from aneurysm lesions compared to cells from the parent artery or the daughter artery were considered to be over-expressed or under-expressed, respectively. A dendrogram was generated using the Morpheus online tool (https://software.broadinstitute.org/morpheus/). All raw RNA-seq data were deposited to the Gene Expression Omni- bus (https://www.ncbi.nlm.nih.gov/geo/) (ID # GSE217440).

Rodent IA models and histological analysis of induced IAs using scanning electron microscopy (SEM)

Seven-week-old male Sprague−Dawley rats were purchased from Japan SLC (Slc: SD, total n = 6, Shizuoka, Japan). The animals were maintained on a light/dark cycle of

12 h/12 h and had free access to food and water.

Anesthesia was induced in rats by the inhalation of Isoflurane (induction; 5.0 %, maintenance; 1.5~2.0 %, #IYESC-0001, Pfizer Inc., New York, NY). Then, IAs were induced by ligation of the left common carotid artery and systemic hypertension, which was achieved by combining a high salt diet and left renal artery ligation [17]. Immediately after the surgical manipulations, animals were fed food containing 8 % sodium chloride and 0.12 % 3-aminopropionitrile (#A0408, Tokyo Chemical Industry, Tokyo, Japan), an inhibitor of lysyl oxidase which catalyzes collagen and elastin crosslinking.

Fourteen days after surgery, the animals were deeply anesthetized with Isoflurane (5.0 %, #IYESC-0001, Pfizer Inc.) and were transcardially perfused with 4 % paraformaldehyde solution for fixation. The bifurcation site of the right anterior cerebral artery (ACA) and olfactory artery (OA), including the induced IA lesions, was stripped and fixed in 2 % glutaraldehyde and 2 % paraformaldehyde solution. The specimens were sequentially treated with 2 % OsO_4 and 1.5 % potassium ferricyanide solution, 1 % thiocarbohydrazine solution, 2 % aqueous OsO_4 solution, and lead aspartate solution. After dehydration, the specimens were embedded in Quetol 812 epoxy resin (Nisshin EM, Tokyo, Japan) containing Ketjen black powder (LION SPECIALTY CHEMICALS CO., LTD, Tokyo, Japan). SEM images were acquired using a Merlin scanning electron

microscope (Carl Zeiss, Gottingen, Germany) equipped with a 3D View in-chamber ultra-microtome system (Gatan, Pleasanton, CA).

Immunohistochemistry for human specimens or HUAECs

Dissected human specimens were fixed in formalin solution and embedded in paraffin. Thick slices (4 μm) were then prepared for immunohistochemical analyses. The slices were deparaffinized in xylene and hydrated in a graded alcohol series. Then, the slices were immersed in antigen retrieval solution (#S1699, DAKO, Agilent Technologies, Santa Clara, CA) and autoclaved for antigen retrieval. After blocking with 10 % donkey serum (#017-000-121, Jackson ImmunoResearch, West Grove, PA) for 1 h at room temperature, the slices were incubated with primary antibodies in phosphate-buffered saline (pH 7.4) at 4 °C over-night, followed by incubation with secondary antibodies conjugated with fluorescence dye in phosphate-buffered saline (pH 7.4) for 1 h at room temperature (Jackson ImmunoResearch). In experiments using HUAECs, cells were cultured on a chamber slide (#354631, Corning, Corning, NY) and fixed with 4 % paraformaldehyde. The slides were blocked with 3 % donkey serum (#017-000-121, Jackson ImmunoResearch) and immunostained as described for human specimens. Finally, fluorescent images were acquired using a confocal fluorescence microscope

(FV3000, Olympus, Tokyo, Japan).

The primary antibodies used were mouse monoclonal anti-CD31 antibody (#M0823, Dako), rabbit polyclonal anti-phosphorylated endothelial nitric oxide synthase (phospho-eNOS) antibody (#PA5-104858, Thermo Fisher Scientific, Waltham, MA), and rabbit polyclonal anti-VE-Cadherin antibody (#28644, Santa Cruz Biotechnology, Dallas, TX). The secondary antibodies used were Alexa Fluor 488-conjugated donkey anti-mouse IgG H&L antibody (#A21202, Thermo Fisher Scientific) and Alexa Fluor 647-conjugated donkey anti-rabbit IgG H&L antibody (#A31573, Thermo Fisher Scientific).

Results

RNA-seq of endothelial cells cultured on the 3D-casted mold after perfusion load

A 3D-casted mold of a human IA lesion located at the middle cerebral artery bifurcation and the surrounding vasculature was made using hydrophilic silicon to enable cell culture on the cast surface (Fig. 1A and B). HUVECs were cultured on the inner cast surface, coated with type I collagen (Fig. 1C-E). The cells were exposed to pulsatile flow that mimicked physiological conditions. The endothelial cells were then fixed, harvested, and analyzed by RNA-seq to identify changes in the gene expression profile in each part of the IA lesion compared to the parent or the daughter artery (Fig. 2A). The locations

where the endothelial cells were harvested are shown in Fig. 2B. Approximately 100 cells were present in each sample.

The mapped read count was about 28 thousand per sample (on average). We identified the differentially expressed genes between groups. Principal component analysis showed that the endothelial cells of the IA lesion clustered differently from cells from the parent artery or the daughter artery in the coordinate axis (Fig. 2A). These results suggest a similar gene expression profile among endothelial cells from each part of the lesion and notably different gene expression patterns between endothelial cells in the IA lesion and control arterial walls. Dendrogram analysis demonstrated a similar gene expression profile among the five specimens from different parts of the IA lesions (Fig. 2C). In contrast, gene expression profiles from the parent or the daughter arteries differed from each other both in principal component analysis and in the dendrogram. These results indicate that hemodynamic force-loading differs in each part of the arterial walls. The gene expression profile in one specimen from the daughter artery (indicated by ‘artery 2’) was similar to that in cells on the IA dome (Fig. 2A and C), presumably due to the similar hemodynamic loading. This occurrence can also be explained by the fact that ‘artery 2’ is the outlet from the dome in computational fluid dynamic analysis.

We identified 1,819 under-expressed genes in IA lesions compared to control arterial

walls (Supplementary Data Table S1). Notably, no genes were identified as over-expressed in IA lesions, suggesting that IA is a relatively silent (not active) lesion. GO terms implying endothelial cell malfunction were determined by analyzing the under-expressed genes in IA lesions. These terms included 'Cellular response to stress' , 'Establishment of localization in cell' , 'Intracellular transport' , and 'Cellular protein-containing complex assembly' in Biological Process (Table 1). 'Inner mitochondrial membrane protein complex' , 'Respiratory chain complex' , 'Mitochondrial respirasome' , and 'Catalytic complex' comprised the Cellular Component (Table 2). At the same time, 'RNA binding' , 'Cadherin binding' , 'Electron transfer activity' , and 'Cell adhesion molecule binding' were identified in Molecular Function (Table 3). Significantly under-expressed genes in cells from the IA dome (compared with those in control arterial walls) included claudin5 (*CLDN5*), Cingulin-like protein 1 (*CGNL1*), and Cadherin5 (*CDH5,* also known as VE-Cadherin). These genes are related to tight junction formation, junction assembly, or adhesion between endothelial cells. We also detected eNOS (*NOS3*), which is related to endothelial cell function (Supplementary Data Table S1), suggesting endothelial cell dysfunction in lesions. Intriguingly, genes under-expressed in endothelial cells in the lesion included those related to mitochondria, such as *HSPD1* (Hsp60) and *COX4I1* (Cytochrome C Oxidase Subunit 4I1) (Supplementary Data Table S1), further

supporting endothelial cell malfunction in lesions.

Endothelial cells damage and malfunction in IA lesions

Based on the results from the comprehensive gene expression profile analysis, we next examined whether endothelial cells in the lesions were indeed dysfunctional. Here, we used SEM to examine the histopathological features of endothelial cells in lesions induced in rats. We observed electron-dense tight junctions between endothelial cells in control intracranial arterial walls. These junctions were almost completely disrupted in IA lesions (Fig. 3), similar to observations in previous studies [18-20]. To explore whether the endothelial cell damage in IA lesions influenced the cellular characteristics, the expression of endothelial cell markers CD31 or VE-Cadherin in IA lesions and control arterial walls was examined using immunohistochemistry. We found that CD31 or VE-Cadherin was expressed in most inner cells, endothelial cells, in control arterial walls (Fig. 4A and B). These markers were significantly reduced and were only weakly detected in cells in IA lesions (Fig. 4A and B), suggesting a loss of endothelial cell character. Furthermore, the expression of the phosphorylated form of eNOS, which reflects endothelial cell function, was also remarkably reduced in the endothelial cells from IA lesions (Fig. 4C). These results suggest that endothelial cells in the lesions are

malfunctioning.

Discussion

We observed endothelial cell malfunction in IA lesions in experiments using a 3D-casted mold. Histopathological examinations of human IA lesions by SEM and immunohistochemistry support these observations. Consistently, previous studies have described an abnormal shape or malfunction exclusively in IA lesions, such as detached cells or disrupted endothelial cell junctions [18-23]. A recent study using a 3D-casted mold combined with quantitative RT-PCR analyses demonstrated that eNOS is under-expressed in endothelial cells in lesions [24], indicating their malfunction. Our results provide evidence that the pathological flow conditions in the IA lesion dome directly disturb endothelial cell function, such as the blood-brain barrier.

Our data failed to identify genes reflecting chronic inflammatory responses, such as those over-expressed in lesions. Because chronic inflammatory responses are considered the major mechanism regulating IA initiation, progression, or rupture [10, 25-33], our results require some explanations. Most unruptured IA lesions are stable and do not rupture or enlarge during follow-up. Thus, the absence of inflammatory responses in endothelial cells in lesions in the present study of unruptured lesions could be explained

by the nature of unruptured IAs (i.e. silent lesions). Another possibility is that inflammatory responses in endothelial cells in lesions triggered by pathological hemodynamic forces require cross-talk with other cell types, such as infiltrating macrophages or adjoining smooth muscle cells. In addition to defective cross-talk among cells other than endothelial cells in the arterial wall, experiments using a 3D-casted mold lack the important hemodynamic factor strain stress in response to heartbeats. If endothelial cells in lesions are activated or maintained under this hemodynamic condition concomitant with shear stress and/or turbulence, our results may indicate that strain stress is an indispensable factor for evoking or maintaining inflammatory responses, in addition to non-physiological WSS or disturbed flow. Furthermore, additional analyses, such as single-cell analysis, may be necessary, particularly if only a small number of cells respond to hemodynamic forces to drive IA initiation, progression, or rupture.

Acknowledgements

We thank all our technical staff and secretaries for their kind assistance. We also thank Editage (www.editage.com) for English language editing.

Source of Funding

This work was supported by Core Research for Evolutional Science and Technology (CREST) on Mechanobiology from the Japan Agency for Medical Research and Development (AMED) (grant ID; JP18gm0810006, JP19gm0810006, JP20gm0810006, T.A.), the grant from AMED (grant ID; JP21ek0210148, H.K.) and by Grant-in-Aid for Scientific Research from The Ministry of Education, Culture, Sports, Science and Technology (grant ID; 20K09381, T.A. and 20K09367, H.K.).

Disclosures

The authors declare that there are no potential conflicts of interest.

Figure Legends

FIGURE 1. 3D-casted model of human unruptured intracranial aneurysm lesion at middle cerebral artery bifurcation.

(A, B) The morphological image of 3D rotational angiography from human case with intracranial aneurysm at the middle cerebral artery bifurcation **(A)** and the image of 3D-casted mold of this lesion made by hydrophilic silicon **(B)**. **(C)** The macroscopic image of the primary culture of endothelial cells from human umbilical artery (HUAECs) is shown in the left panel. On the right, the images of immunofluorescent staining of

HUAECs for endothelial cell markers, CD31 (green) and VE-Cadherin (red), nuclear staining by DAPI (blue), or merged images are shown. The images from immunofluorescent staining without primary antibodies are served to show negative control experiments and are shown in the lower panels. Scale bar: 50 μm. **(D)** Culture of HUAECs on the surface of hydrophilic silicon-made 3D-casted mold. The images of the surface of 3D-casted mold are shown. The square in the left panel indicates the region where the images were acquired. **(E)** The representative view of the experimental apparatus to expose hemodynamic force to endothelial cells cultured on the inner surface of the 3D-casted model.

FIGURE 2. Comprehensive gene expression profile analysis of endothelial cells cultured on 3D-casted mold.

(A) The principal component analysis of comprehensive gene expression profile data from endothelial cells on the dome of intracranial aneurysm lesion (Aneurysm), the parent or the daughter artery (Artery). **(B)** The macroscopic image of 3D-casted mold to indicate the regions where endothelial cells were harvested. The squares in white or black color indicate the regions classified as ‘artery’ or ‘aneurysm’, respectively. **(C)** The heat map showing gene expression profile of under-expressed genes in endothelial cells on the

dome (Aneurysm) compared with the profile in cells on the parent or the daughter artery (Artery). Dendrogram is also provided.

FIGURE 3. Disruption of the tight junction between endothelial cells in intracranial aneurysm lesions induced in rats.

Disruption of the tight junction between endothelial cells in intracranial aneurysm (IA) lesions induced in rats revealed by scanning electron microscopic examination. IA lesions induced in a rat model were harvested before (Day 0) or on the 14^{th} day after the surgical manipulations (Day 14) and subjected to histopathological examinations by scanning electron microscopy. Magnified images corresponding to the squares in the left panels are shown on the right. The asterisk indicate the lumen side. The white arrow head or black ones in the upper panel indicate the electron-dense tight junction or attachment between endothelial cells (ECs), respectively. The black arrow in the lower panel indicates the disruption of the barrier between ECs. Scale bar: 10 μm.

FIGURE 4. Reduced expression of endothelial cell markers or phosphorylated form of eNOS in human intracranial aneurysm lesions.

Expression of CD31 **(A)**, VE-Cadherin **(B)** or phosphorylated form of endothelial nitric

oxide synthase (Phospho-eNOS) **(C)** in human intracranial aneurysm lesions and control arterial walls (superficial temporal artery). The images of immunofluorescent staining of the lesions or control arterial walls for CD31 (green in **A**), VE-Cadherin (green in **B**), phosphorylated form of eNOS (green in **C**), nuclear staining by DAPI (blue) or merged images are shown. Magnified images corresponding to the squares in the left panels are shown on the right. The asterisk indicates the lumen side. The images from immunofluorescent staining without primary antibodies serve to show negative control experiments and are shown on the right. Scale bar: 50 μm.

Table 1. Down-represented terms in gene ontology analysis (Biological Process).

Table 2. Down-represented terms in gene ontology analysis (Cellular Component).

Table 3. Down-represented terms in gene ontology analysis (Molecular Function).

Supplementary Data Table S1. The list of under-expressed genes in endothelial cells in the dome of the aneurysm.

References

1. Wiebers D.O., Piepgras D.G., Brown R.D., Jr., et al. Unruptured aneurysms. J Neurosurg 2002;96:50-1; discussion 58-60
2. van Gijn J., Kerr R.S., Rinkel G.J. Subarachnoid haemorrhage. Lancet 2007;369:306-18
3. Rinkel G.J., Djibuti M., Algra A., et al. Prevalence and risk of rupture of intracranial aneurysms: a systematic review. Stroke 1998;29:251-6
4. Lawton M.T., Vates G.E. Subarachnoid Hemorrhage. N Engl J Med 2017;377:257-66
5. Brisman J.L., Song J.K., Newell D.W. Cerebral aneurysms. N Engl J Med 2006;355:928-39
6. Morita A., Kirino T., Hashi K., et al. The natural course of unruptured cerebral aneurysms in a Japanese cohort. N Engl J Med 2012;366:2474-82
7. Aoki T., Nishimura M., Matsuoka T., et al. PGE(2) -EP(2) signalling in endothelium is activated by haemodynamic stress and induces cerebral aneurysm through an amplifying loop via NF-kappaB. Br J Pharmacol 2011;163:1237-49
8. Aoki T., Yamamoto K., Fukuda M., et al. Sustained expression of MCP-1 by low wall shear stress loading concomitant with turbulent flow on endothelial cells of intracranial aneurysm. Acta Neuropathol Commun 2016;4:48
9. Dolan J.M., Kolega J., Meng H. High wall shear stress and spatial gradients in vascular pathology: a review. Ann Biomed Eng 2013;41:1411-27
10. Frosen J., Cebral J., Robertson A.M., et al. Flow-induced, inflammation-mediated arterial wall remodeling in the formation and progression of intracranial aneurysms. Neurosurg Focus 2019;47:E21
11. Jou L.D., Lee D.H., Morsi H., et al. Wall shear stress on ruptured and unruptured intracranial aneurysms at the internal carotid artery. AJNR Am J Neuroradiol 2008;29:1761-7
12. Shojima M., Oshima M., Takagi K., et al. Magnitude and role of wall shear stress on cerebral aneurysm: computational fluid dynamic study of 20 middle cerebral artery aneurysms. Stroke 2004;35:2500-5
13. Turjman A.S., Turjman F., Edelman E.R. Role of fluid dynamics and inflammation in intracranial aneurysm formation. Circulation 2014;129:373-82
14. Ishida F., Tsuji M., Tanioka S., et al. Computational Fluid Dynamics for Cerebral Aneurysms in Clinical Settings. Acta Neurochir Suppl 2021;132:27-32
15. Soldozy S., Norat P., Elsarrag M., et al. The biophysical role of hemodynamics in the pathogenesis of cerebral aneurysm formation and rupture. Neurosurg Focus

2019;47:E11

16. Murayama Y., Fujimura S., Suzuki T., et al. Computational fluid dynamics as a risk assessment tool for aneurysm rupture. Neurosurg Focus 2019;47:E12
17. Aoki T., Miyata H., Abekura Y., et al. Rat Model of Intracranial Aneurysm: Variations, Usefulness, and Limitations of the Hashimoto Model. Acta Neurochir Suppl 2020;127:35-41
18. Scanarini M., Mingrino S., Zuccarello M., et al. Scanning electron microscopy (s.e.m.) of biopsy specimens of ruptured intracranial saccular aneurysms. Acta Neuropathol 1978;44:131-4
19. Yamamoto R., Aoki T., Koseki H., et al. A sphingosine-1-phosphate receptor type 1 agonist, ASP4058, suppresses intracranial aneurysm through promoting endothelial integrity and blocking macrophage transmigration. Br J Pharmacol 2017;174:2085-101
20. Koseki H., Miyata H., Shimo S., et al. Two Diverse Hemodynamic Forces, a Mechanical Stretch and a High Wall Shear Stress, Determine Intracranial Aneurysm Formation. Transl Stroke Res 2020;11:80-92
21. Jamous M.A., Nagahiro S., Kitazato K.T., et al. Endothelial injury and inflammatory response induced by hemodynamic changes preceding intracranial aneurysm formation: experimental study in rats. J Neurosurg 2007;107:405-11
22. Tamura T., Jamous M.A., Kitazato K.T., et al. Endothelial damage due to impaired nitric oxide bioavailability triggers cerebral aneurysm formation in female rats. J Hypertens 2009;27:1284-92
23. Sheinberg D.L., McCarthy D.J., Elwardany O., et al. Endothelial dysfunction in cerebral aneurysms. Neurosurg Focus 2019;47:E3
24. Levitt M.R., Mandrycky C., Abel A., et al. Genetic correlates of wall shear stress in a patient-specific 3D-printed cerebral aneurysm model. J Neurointerv Surg 2019;11:999-1003
25. Aoki T., Kataoka H., Shimamura M., et al. NF-kappaB is a key mediator of cerebral aneurysm formation. Circulation 2007;116:2830-40
26. Aoki T., Frosen J., Fukuda M., et al. Prostaglandin E2-EP2-NF-kappaB signaling in macrophages as a potential therapeutic target for intracranial aneurysms. Sci Signal 2017;10:eaah6037
27. Aoki T., Kataoka H., Ishibashi R., et al. Impact of monocyte chemoattractant protein-1 deficiency on cerebral aneurysm formation. Stroke 2009;40:942-51
28. Kanematsu Y., Kanematsu M., Kurihara C., et al. Critical roles of macrophages in the formation of intracranial aneurysm. Stroke 2011;42:173-8

29. Aoki T., Narumiya S. Prostaglandins and chronic inflammation. Trends Pharmacol Sci 2012;33:304-11
30. Chyatte D., Bruno G., Desai S., et al. Inflammation and intracranial aneurysms. Neurosurgery 1999;45:1137-46; discussion 46-7
31. Frosen J., Piippo A., Paetau A., et al. Remodeling of saccular cerebral artery aneurysm wall is associated with rupture: histological analysis of 24 unruptured and 42 ruptured cases. Stroke 2004;35:2287-93
32. Fukuda M., Aoki T. Molecular basis for intracranial aneurysm formation. Acta Neurochir Suppl 2015;120:13-5
33. Shimizu K., Kushamae M., Mizutani T., et al. Intracranial Aneurysm as a Macrophage-mediated Inflammatory Disease. Neurol Med Chir (Tokyo) 2019;59:126-32

Figure 1

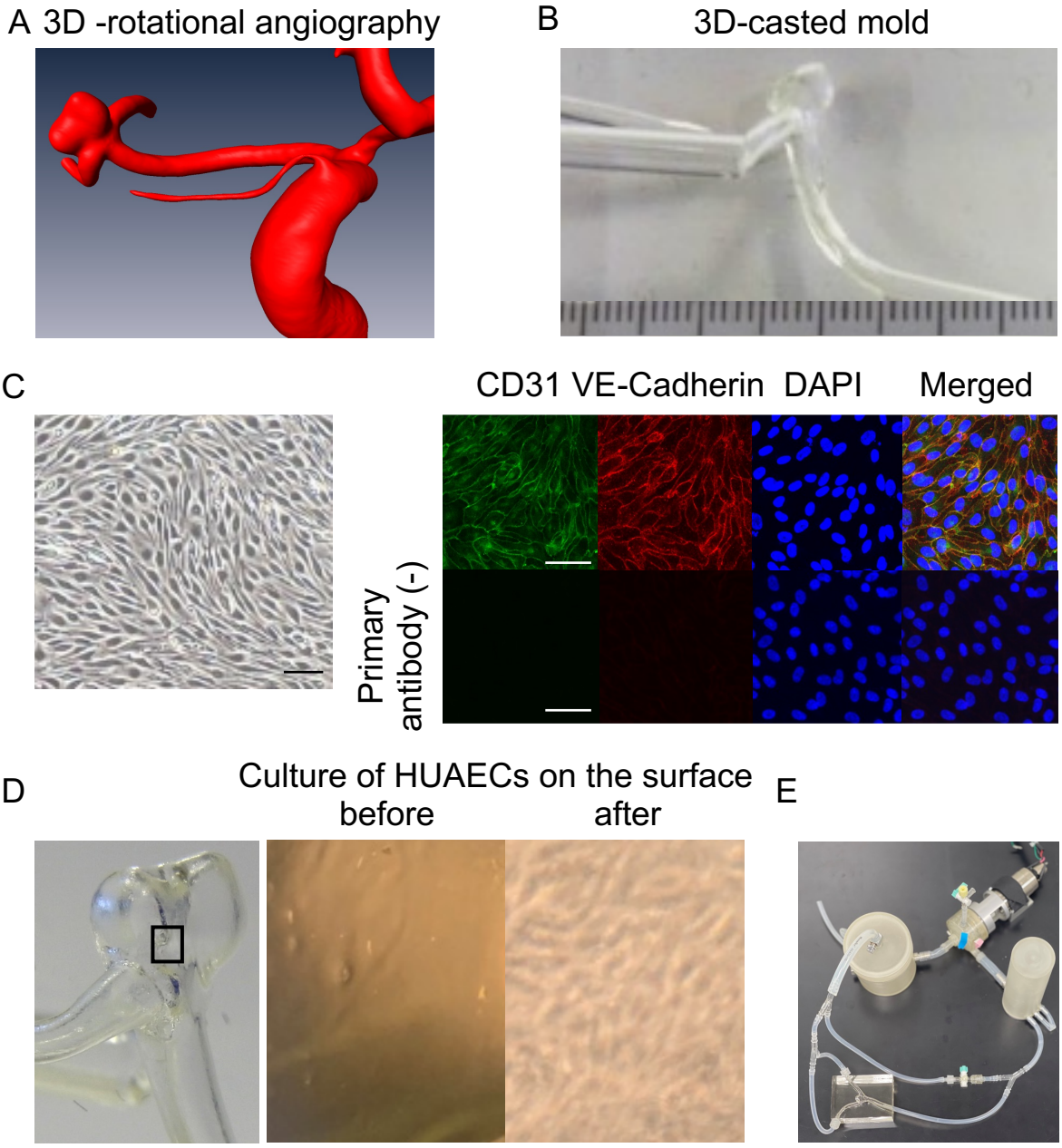
A 3D -rotational angiography
B
3D-casted mold
C
CD31 VE-Cadherin DAPI Merged
Primary antibody (-)
D
Culture of HUAECs on the surface
before
after
E

Figure 2

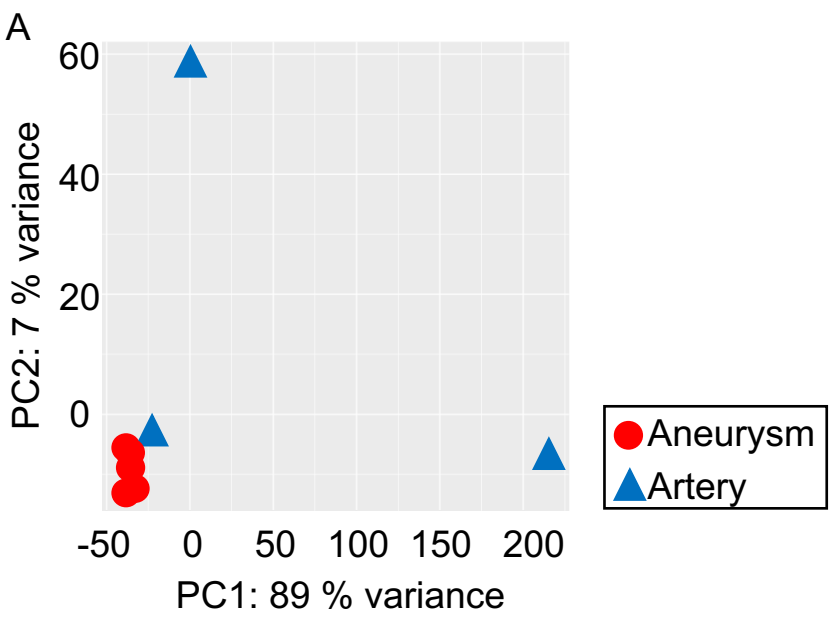
A
60
40
20
0
PC2: 7 % variance
-50
0
50
100
150
200
PC1: 89 % variance
Aneurysm
Artery

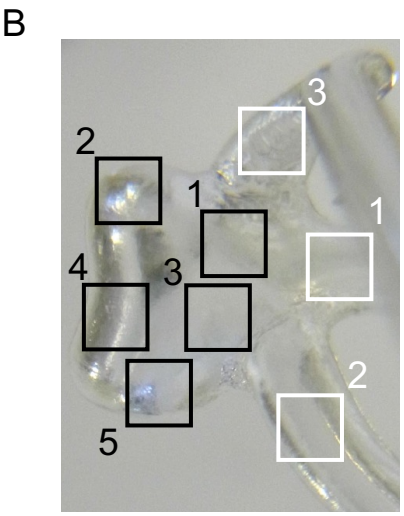
B
3
2
1
1
4
3
2
5

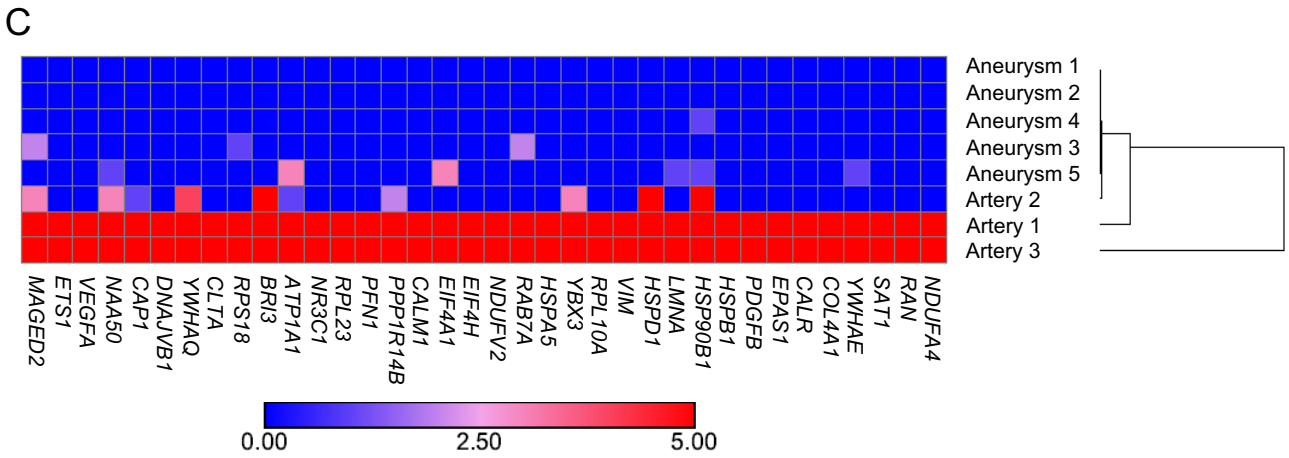
C
Aneurysm 1
Aneurysm 2
Aneurysm 4
Aneurysm 3
Aneurysm 5
Artery 2
Artery 1
Artery 3
MAGED2
ETS1
VEGFA
NAA50
CAP1
DNAJVB1
YWHAQ
CLTA
RPS18
BRI3
ATP1A1
NR3C1
RPL23
PFN1
PPP1R14B
CALM1
EIF4A1
EIF4H
NDUFV2
RAB7A
HSPA5
YBX3
RPL10A
VIM
HSPD1
LMNA
HSP90B1
HSPB1
PDGFB
EPAS1
CALR
COL4A1
YWHAE
SAT1
RAN
NDUFA4
0.00
2.50
5.00

Figure 3

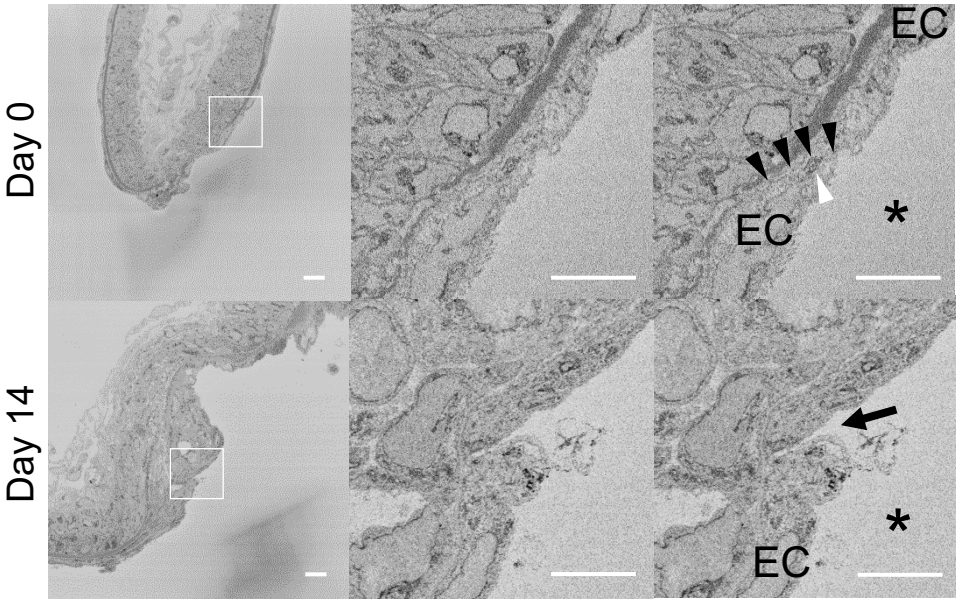

Figure 4

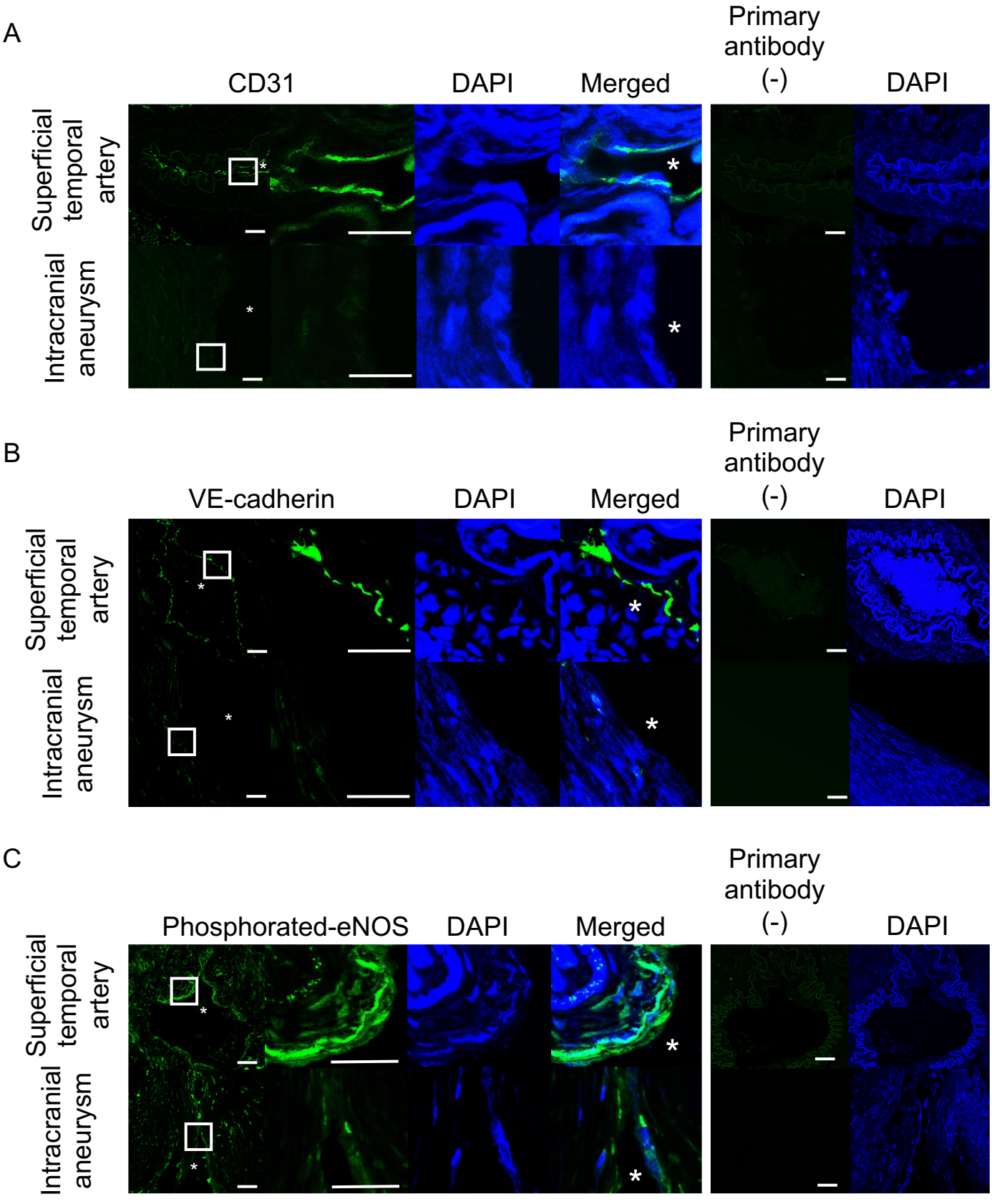
A
CD31
DAPI
Merged
Primary antibody (-)
DAPI
Superficial temporal artery
Intracranial aneurysm
B
VE-cadherin
DAPI
Merged
Primary antibody (-)
DAPI
Superficial temporal artery
Intracranial aneurysm
C
Phosphorated-eNOS
DAPI
Merged
Primary antibody (-)
DAPI
Superficial temporal artery
Intracranial aneurysm

Table 1. Down-represented terms in gene ontology analysis (Biological Process).

GO term	P-value
Cellular response to stress	2.60E-08
Establishment of localization in cell	1.30E-07
Cellular macromolecule catabolic process	1.30E-06
Intracellular transport	1.50E-06
Macromolecule catabolic process	2.80E-06
Cellular protein-containing complex assembly	2.80E-06
Protein-containing complex subunit organization	2.80E-06
MRNA metabolic process	5.30E-06
Ubiquitin-dependent protein catabolic process	7.60E-06
Apoptotic process	7.60E-06
Response to organic substance	7.60E-06
Protein catabolic process	7.60E-06
Modification-dependent macromolecule catabolic process	8.80E-06
Modification-dependent protein catabolic process	1.10E-05
Proteasomal protein catabolic process	1.20E-05

Table 2. Down-represented terms in gene ontology analysis (Cellular Component).

Go term	P-value
Nucleoplasm	4.60E-10
Nuclear lumen	4.50E-09
Vesicle	1.10E-07
Extracellular exosome	1.10E-07
Extracellular organelle	1.50E-07
Inner mitochondrial membrane protein complex	7.20E-07
Respiratory chain complex	3.60E-06
Mitochondrial respirasome	5.40E-06
Catalytic complex	9.70E-06
Mitochondrial protein-containing complex	1.10E-05
Organelle membrane	1.70E-05
Organelle envelope	2.00E-05
Respirasome	2.00E-05

Table 3. Down-represented terms in gene ontology analysis (Molecular Function).

Go term	P-value
RNA binding	1.00E-08
Enzyme binding	3.40E-06
Cadherin binding	7.90E-06
Nucleic acid binding	8.40E-05
NAD(P)H dehydrogenase (quinone) activity	2.00E-04
Electron transfer activity	2.00E-04
NADH dehydrogenase activity	2.40E-04
Oxidoreductase activity, acting on NAD(P)H, quinone or similar compound as acceptor	2.40E-04
NADH dehydrogenase (quinone) activity	2.40E-04
NADH dehydrogenase (ubiquinone) activity	6.80E-04
Cell adhesion molecule binding	6.80E-04
Proton transmembrane transporter activity	7.30E-04
Oxidoreductase activity, acting on NAD(P)H	8.10E-04
ATPase activity, coupled to transmembrane movement of ions, rotational mechanism	4.00E-03